Microwave Imaging of Biological Tissue Phantom in Different Frequency Ranges

L. N. Anishchenko, I. L. Alborova, M. A. Chizh, and A. V. Zhuravlev
Bauman Moscow State Technical University, Moscow, Russia

Abstract— In the present study the microwave images for the breast tissue phantom in different frequency ranges were obtained. The phantom was made of lard imitating fat breast tissue and dielectrically contrast inclusions. Experimental data were gathered by using the installation consisted of a vector network analyzer, two linear drives, a single transceiving antenna, flexible armored antenna feeders, a microcontroller board, and a computer. Recorded by the vector network analyzer scattered electromagnetic field parameters were further processed utilizing an algorithm written in Python Programming Language to reconstruct microwave image of the inner dielectric inhomogeneities of the phantom.

1. INTRODUCTION

At present breast cancer remains the second leading cause of cancer death in women all over the world. However, the death rate may be greatly decreased by the early diagnosis of this decease. Currently used medical screening methods such as mammography and ultrasound scanning are effective only for already formed tumors. It results in late aggressive tumors detection, which is characterized by high growth speed, when prognosis is not always good. That is why it is up-to-date task to develop methods, which detect not structural but functional changes in biological tissues taking place from the beginning of the oncogenesis. One such method is a microwave imaging, which dates back to the 1970s [1]. During last several decades there is a growing interest in application of microwave imaging method in medicine especially in breast tumors detection [2, 3] and brain disease diagnostics and monitoring [4–6]. The main difficulties in microwave imaging of biological tissue are huge tissue loss, relatively low malignant/healthy tissue contrast and significant variety of the dielectric properties [7, 8]. At present, some of these problems may be overcome by usage of additional contract agents (magnetic nanoparticles) [9, 10]. The main drawback of such approach is that this method no longer remains noninvasive. Another possible way of dealing with this issue is application of additional microwave image processing to enhance the contrast.

2. EXPERIMENTAL INSTALLATION

In present work we compare microwave images of the biological tissue phantom with several inclusions at three frequency ranges: 5.6–6.6, 14–15 and 20–22 GHz with the frequency step of 0.2 GHz. The phantom was made of the pig fat tissue imitating human breast fat tissue (relative permittivity $\varepsilon \approx 5$). Scheme of the phantom is given in Fig. 1. Phantom contains six dielectrically contrast inclusions: three of them were made of material imitating tumor ($\varepsilon \approx 40$) of 10 mm diameter each and three metal balls with diameters 14, 10 and 6 mm. To scan the phantom it was placed on the platform of the mechanical scanner. Scanning procedure was performed for the area of the phantom (21×27 cm) with the step of 3 cm. Scattering parameters were recorded at each of the step points.

The simplified diagram of the used setup and its photo are given in Figs. 2 and 3, respectively. The setup consists of the following components: a vector network analyzer (VNA), two linear drives, a single transceiving antenna, flexible armored antenna feeders, a microcontroller board, and a computer [11].

The antenna is mounted on a wooden arm positioned by the tripod over the scanning plane. A breast tissue phantom is placed on the wooden platform, which can be moved by the two linear drives. To suppress the clutter caused by massive metallic elements of the linear drives a piece of radio-absorbing material may be placed on the platform under the phantom, but in present experiment it is not the case because the scanning area is smaller than the actual size of the phantom.

The VNA is connected to local area network to receive commands from the computer and retrieve the data. Before each measurement cycle, VNA is preconfigured to measure S_{11} parameter on a desired frequency grid. VNA is also configured to start a single sweep by the external signal. The microcontroller board is controlled by the same computer and provides real-time signals to

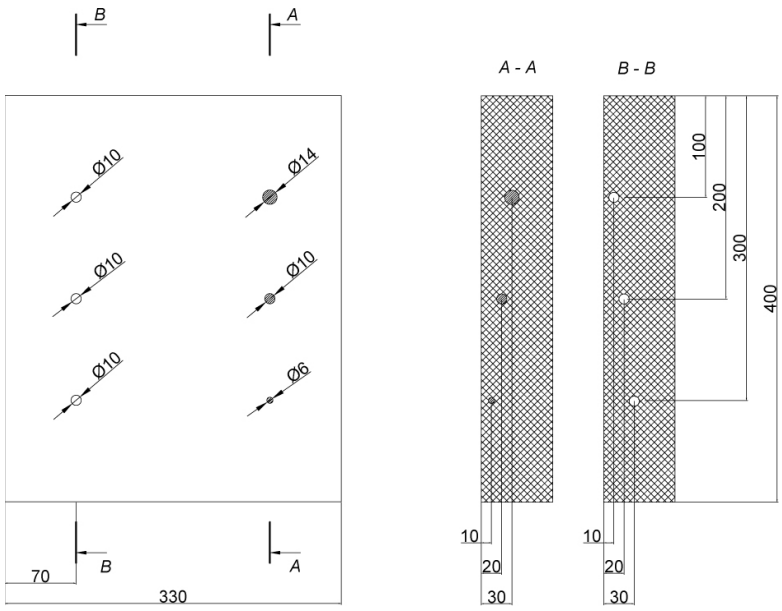

Figure 1: Scheme of the used breast tissue phantom.

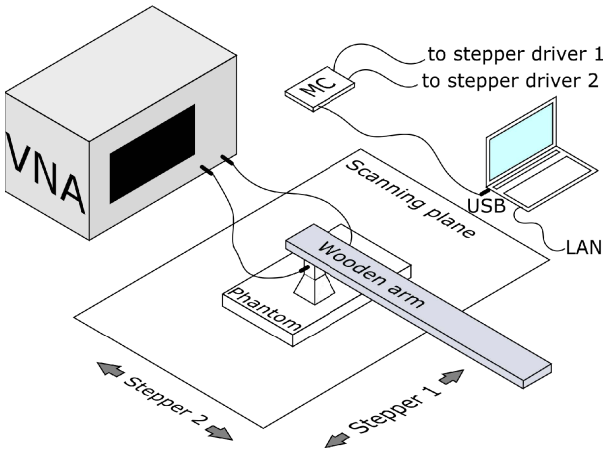

Figure 2: Experimental setup diagram.

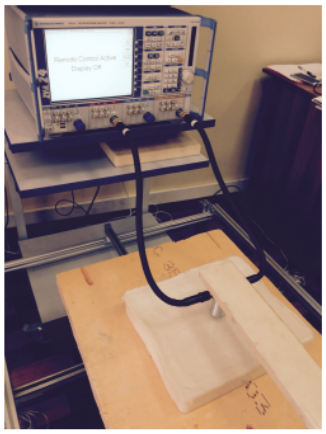

Figure 3: Photo of the experimental setup.

the linear drives, giving the trigger signal to the VNA when the current active linear drive carriage passes a given sampling point. As a microcontroller board we used an Arduino board.

The vector network analyzer is connected to local area network to receive commands from the computer and retrieve the data. Before each measurement cycle, VNA is preconfigured to measure S_{11} parameters on a desired frequency grid. VNA is also configured to start a single sweep by the external signal. The a microcontroller board is controlled by the same computer and provides real-time signals to the linear drives, giving the trigger signal to the VNA when the current active linear drive carriage passes a given sampling point. As a microcontroller board we used an Arduino board.

3. EXPERIMENTAL RESULTS AND IMAGE PROCESSING

Each set of the experimental data may be interpreted as a reflected signal E (complex amplitude). Here we used the processing technique based on plane wave decomposition and back propagation of the obtained two-dimensional Fourier spectrum, which were described in [11]. Fig. 4 presents the results of the phantom scanning at different frequency ranges (for each frequency range one frequency was chosen). Experimental results have shown that inclusion of 6 mm in diameter can be detected only at the frequency ranges of 14.0–15.0 and 21.0–22.0 GHz. As for the depth parameter, the inclusions may be seen for all used in the present experiment frequency ranges up to the depth

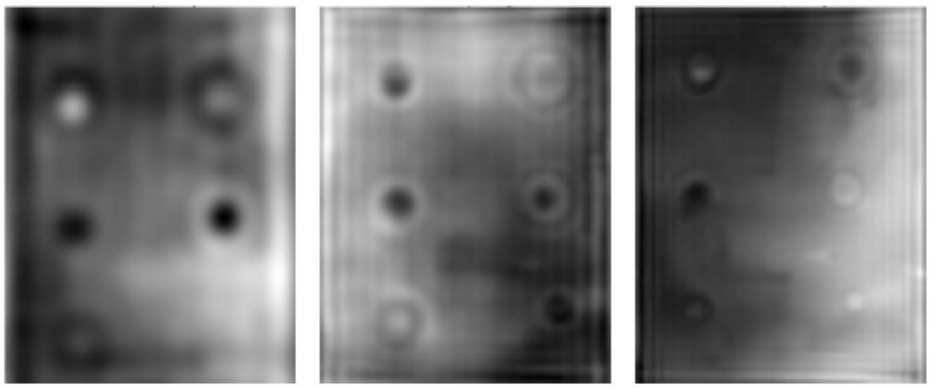

(a) (b) (c)

Figure 4: Experimental results ((a) 5.8 GHz, (b) 14.2 GHz, (c) 21.2 GHz).

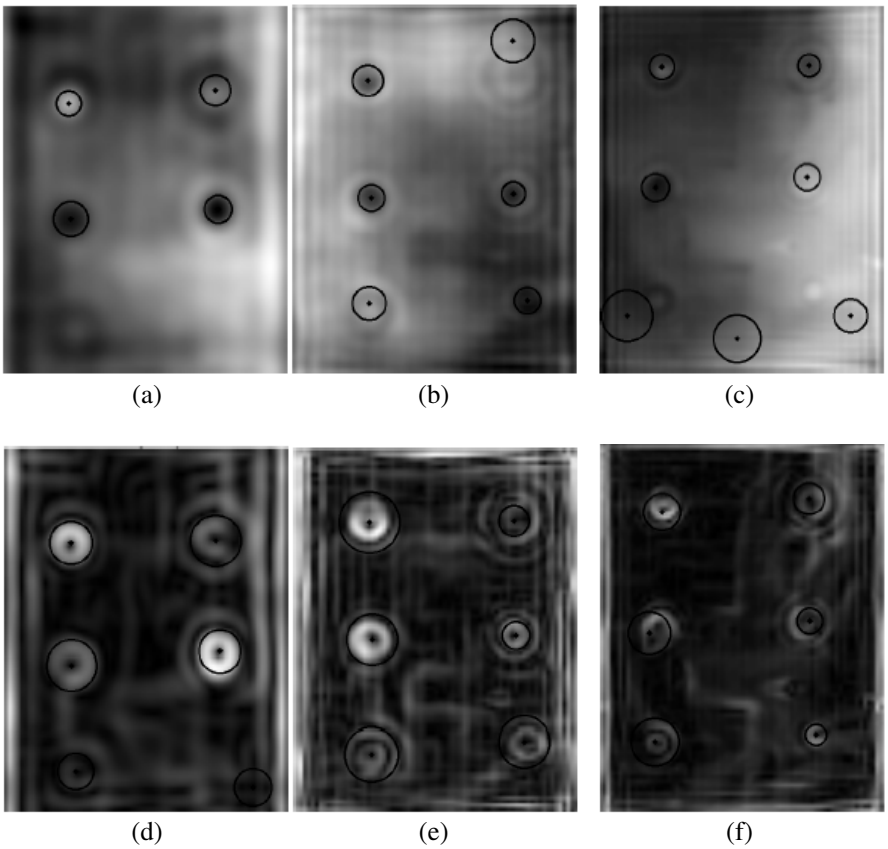

(a) (b) (c)

(d) (e) (f)

Figure 5: Experimental results with detected inclusions ((a), (d) 5.8 GHz, (b), (e) 14.2 GHz, (c), (f) 21.2 GHz, (a), (b), (c) original phase, (d), (e), (f) filtering results).

of 3 cm.

It is worth mentioning that in the current phantom the skin layer as a part of a breast was neglected. Since the skin tissue has high value of dielectric permittivity ($\varepsilon \approx 40$), the presence of the skin layer in a real conditions may result in a smaller value of a maximum depth at which the inclusion can be detected.

To improve the contrast of the image a processing algorithm was written utilizing Python. Different types of filtering procedures were tested and combined: bias removal, subtraction of the mean in rows and columns of the image, median filtration, and several image processing filters from Multi-dimensional image processing package [12].

The best performance showed the following data processing algorithm:

i. Bias removal. It was done by calculating the mean value for the whole image and its subtrac-

tion.

ii. Median filtration. It was applied for noise removals, which is an essential image preprocessing step for further edge detection.

iii. Edge detection. We applied a two dimensional gradient magnitude filter using Gaussian derivatives to perform edge detection. The standard deviations of the Gaussian filter was set equal to 0.5 for both axis of the microwave image. The value of the standard deviation was picked up empirically.

To prove that the proposed processing algorithm increases the contrast of the microwave image we compare the efficiency of the inclusions detection on both original phase images and processed ones. All inclusions in the phantom were spherical or close to spherical. Therefore, for inclusions detection we used Hough Transform to find circles in the images. In Fig. 5 the phase images before and after band-pass Fourier-spectrum filtration for different frequency ranges are given. Localization of the inclusions detected by Hough Transform are shown as black circles. As it can be seen from Fig. 5 inclusions on the images processed by the filtering algorithm are detected better than on the original images. The number of false detections on the processed images has decreased, in most cases all the six inclusion were localized correctly.

4. CONCLUSION

In present paper, microwave images for the specially designed breast tissue phantom in different frequency ranges were obtained. Furthermore, the experimental setup, which was used in data gathering process, was described. Microwave images reconstructed from parameters registered by VNA showed that for all tested frequency ranges dielectric inhomogineties of 1 cm diameter may be detect up-to the depth of 3 cm. Moreover, higher frequencies predictably provide better space resolution (the smallest 6 mm diameter inclusion can be detected only for the frequency ranges 14–15, 21–22 GHz, but not for the lowest of the tested frequency range of 5.6–6.6 GHz). The quality of microwave image of the phantom may be improved by the usage of additional processing steps proposed in the paper.

The main limitation of the phantom usage described in the present study is the neglect of the skin layer presence and not anthropomorphic shape of the phantom. In future work we suppose to use more realistic multilayer breast phantom.

ACKNOWLEDGMENT

This research has been supported by grants of the Russian Science Foundation, project #15-19-30012 (in part of microwave imaging processing) and project #15-19-00129 (in part of experimental setup design).

REFERENCES

1. Larsen, L. E. and J. H. Jacobi, *Medical Applications of Microwave Imaging*, IEEE Press, 1986.
2. Klemm, M., J. A. Leendertz, D. Gibbins, I. J. Craddock, A. Preece, and R. Benjamin, "Microwave radar-based differential breast cancer imaging: Imaging in homogeneous breast phantoms and low contrast scenarios," *IEEE Trans. Antennas Propag.*, Vol. 57, No. 7, 2337–2344, 2010.
3. Bourqui, J., J. M. Sill, and E. C. Fear, "A prototype system for measuring microwave frequency reflections from the breast," *Int. J. Biomed. Imag.*, 12, 2012.
4. Fhager, A., Y. Yinan, T. McKelvey, and M. Persson, "Stroke diagnostics with a microwave helmet," *Proc. of the 7th European Conference on Antennas and Propagation (EuCAP'13)*, 845–846, 2013.
5. Scapaticci, R., O. M. Bucci, I. Catapano, and L. Crocco, "Differential microwave imaging for brain stroke followup," *International Journal of Antennas and Propagation*, Vol. 2014, 11, 2014.
6. Ireland, D. and M. E. Bialkowski, "Microwave head imaging for stroke detection," *Progress In Electromagnetics Research M*, Vol. 21, 163–175, 2011.
7. Lazebnik, M., et al., "A large-scale study of the ultrawideband microwave dielectric properties of normal, benign and malignant breast tissues obtained from reduction surgeries," *Phys. Med. Biol.*, Vol. 52, 2637–2656, 2007.
8. Lazebnik, M., et al., "A large-scale study of the ultra wideband microwave dielectric properties of normal, benign and malignant breast tissue obtained from cancer surgeries," *Phys. Med. Biol.*, Vol. 52, 6093–6115, 2007.

9. Bucci, O. M., L. Crocco, and R. Scapaticci, "On the optimal measurement configuration for magnetic nanoparticles-enhanced breast cancer microwave imaging," *IEEE Transactions on Biomedical Engineering*, Vol. 62, No. 2, 407–414, 2015.
10. Shea, J., P. Kosmas, B. V. Veen, and S. Hagness, "Contrast enhanced microwave imaging of breast tumors: A computational study using 3D realistic numerical phantoms," *Inverse Problems*, Vol. 26, No. 7, 1–22, 2010.
11. Zhuravlev, A., V. Razevig, S. Ivashov, A. Bugaev, and M. Chizh, "Experimental simulation of multi-static radar with a pair of separated movable antennas," *IEEE International Conference on Microwaves, Communications, Antennas and Electronic Systems*, Tel Aviv, Israel, Nov. 2015.
12. http://docs.scipy.org/doc/scipy/reference/ndimage.html.